Available online at www.sciencedirect.com

ScienceDirect

Journal of Magnesium and Alloys 11 (2023) 4485–4497

www.elsevier.com/locate/jma

Full Length Article

Embryo-to-lamella transition of grain boundary twins in magnesium

Mariyappan Arul Kumar[a,*], Irene J Beyerlein[b]

[a] *Materials Science and Technology Division, Los Alamos National Laboratory, Los Alamos, NM 87545, USA*
[b] *Mechanical Engineering Department, Materials Department, University of California, Santa Barbara, CA 93106, USA*

Received 14 December 2022; received in revised form 28 May 2023; accepted 23 June 2023
Available online 11 August 2023

Abstract

A combined experimental and computational analysis is performed to investigate the less commonly studied embryo-to-lamella transition of deformation twins in magnesium. This work aims to understand the structural variables controlling the embryo-to-lamella transition from grain boundaries. Statistical analysis of hundreds of early-stage twins in the lightly deformed microstructure reveals a prevailing wedge shape, with a much thicker base along the grain boundary (GB) where they originate and a thinner tip terminating in the crystal. The analysis also shows that the GB base is super thick and identifies a minimum GB twin thickness among all early-stage twins that is about one micron. A crystal plasticity-based full-field model is employed to calculate the driving forces to migrate the boundary of a three-dimensional GB twin embryo. The stress analysis, considering a full range of embryo shapes and neighboring grain orientations, indicate that the twin embryo is most likely going to form a wedge shape when it first propagates. The calculations predict that the thickness of the embryo at the GB needs to be significantly larger than its length into the crystal in order to propagate into the crystal. The analysis finds that the more aligned the twin embryo variant is with basal slip in the neighboring grain, the thinner the twin embryo needed for propagation.

Keywords: Magnesium; Twin embryo; Crystal plasticity; Nucleation; Grain neighbor.

1. Introduction

Hexagonal close packed (HCP) magnesium and its alloys deform as easily by deformation twinning as by slip, which distinguishes them from the more common cubic crystals (both face-centered (FCC) and body-centered (BCC)) [1–3]. At the mesoscopic scales, twins in HCP crystals are recognized as plate-like lamellae, lenticular or planar in cross section, that often span the entire crystal [4–11]. Hence, twins can grow to be as large as the crystal itself. Twins shear the crystal by a specific amount [3]. This distinct shearing action re-positions the atoms in a certain way, resulting in a new lattice orientation, that is the characteristic of the twin as well [12,13]. As a result, the crystal, surrounding the twin, becomes locally sheared, and it gains a twin/matrix boundary, which delineates the twin-reoriented domain from the original crystal [4,9,12,13]. Undoubtedly, HCP twins profoundly alter the microstructure, deformation response (strength), and functional properties of their parent crystal relative to the untwinned state [14–18]. For this reason, HCP twins have been and continue to be intensely researched and questions regarding which twins form, why they form, and where they form have yet to be clarified.

Yet although a common mechanism, HCP twinning is not as well understood compared to slip or deformation twinning in simpler FCC and BCC crystals. The study of HCP twinning is complicated by the fact that twin formation involves several steps at distinct length scales. It begins with the initial atomic-scale defect that transforms into the first twin embryo [19–23], is followed by the extension of an embryo into a submicron-size lamella, and then after fully spanning the grain, thickens and/or crosses the boundaries of its own parent [4-6,24-28]. Over the years, every step in this process has received attention analytically and numerically [22,23,25,29-35], and experimentally [4-6,9,36-44].

* Corresponding author.
E-mail address: marulkr@gmail.com (M.A. Kumar).

https://doi.org/10.1016/j.jma.2023.06.003

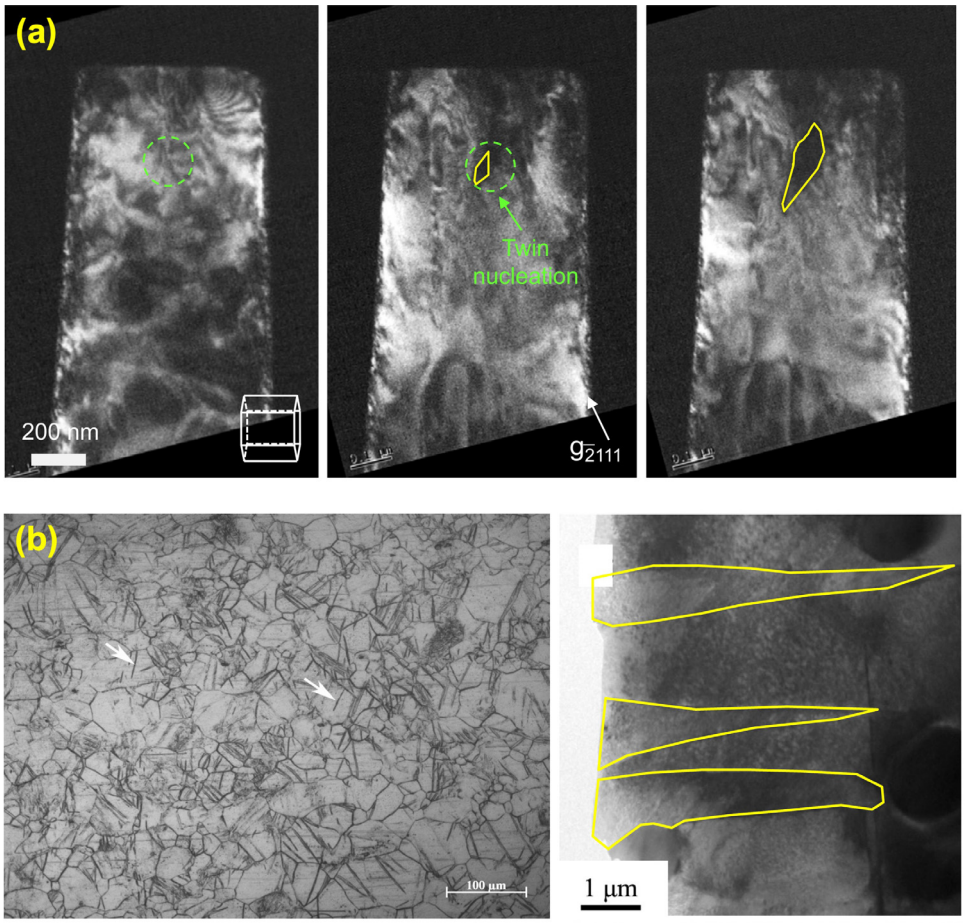

Fig. 1. Microscopy evidence of embryonic and wedge shape twins in Mg. (a) In-situ TEM reveals the formation of a $\{10\bar{1}2\}$ tensile twin embryo at the junction of prismatic ⟨a⟩ slip and basal stacking faults in high pure Mg, followed by the development of an embryonic twin, marked in yellow [9]. (b) TEM images show wedge-shape $\{10\bar{1}2\}$ tensile twins in hot rolled Mg-Gd-Y-(Ag)-Zr alloy [48]. Figures are reproduced with permission from the publishers.

The one step that has in fact received the least attention is the one that controls when a twin transitions from the embryo to the submicon-size lamella. In Transmission Electron Microscopy (TEM) studies of many different kinds of HCP metals, twin embryos are found in a seed-like shape [9,20,45-48]. They all bear the characteristic twin/matrix orientation relationship at the boundary and their boundaries, being curved, are comprised of connected B/P (Basal/Prismatic) facets, P/B (Prismatic/Basal) facets, and coherent twin boundary (CTB) segments [49–53]. Although observations find that these embryos vary widely in size, they are not just a few atomic planes thick (as in FCC and BCC twins) but in fact several tens to hundreds of atomic planes thick or nm in dimension.

As an example, $\{10\bar{1}2\}$ tensile twin nucleation in single crystal Mg is shown in Fig. 1(a), in which a twin embryo is seen to nucleate at the junction of prismatic ⟨a⟩ slip and basal stacking faults [9]. When first detected, it was a few tens of nm in size. Later under further straining, the twin embryo is seen to extend anisotropically from an ellipsoid to a more planar-like shape. Atomic-scale simulations have sought to determine the minimum number of twin planes needed for a twin embryo to be stable under zero stress, and they have suggested that the critical size is not just a few, but 17 atomic planes, at least in the case for the most common HCP twin $\{10\bar{1}2\}\langle\bar{1}011\rangle$[49]. For an embryo in the GB, atomistic and analytical models find it to be much smaller, just three to five atomic planes [54]. The fact that twin lamellae begin as embryos several nm in size distinguishes them from slip and from twinning in simpler structured crystals (e.g., FCC). Yet still, the stable embryo size proposed from simulation and theory is still finer, by an order of magnitude, than the size detected via microscopy. The transitions from a stable twin embryo to a growing embryo to a submicron-size lamella are not well understood. Understanding such transitions is paramount. Twins can only shear the crystal by a characteristic amount per twin plane, so for twin embryos to become effective deformation mechanisms for their parent crystal, they need to increase in volume.

Twin growth involves migrating the twin boundary into perfect crystal and that this process is usually driven by stress [24,25,34,55,56]. Given its typical ellipsoidal-like shape it can either grow laterally, normal to the twin plane, or transversely, along the twin plane, extending into the elongated twin lamella, the shape that is often seen, or both. Growth of twin embryo would involve the migration of defects on the boundary, the P/B and B/P facets and twinning

disconnections. Recently, using atomistic calculations, a few studies clearly demonstrated the role of disconnections on the twin/matrix boundary on the growth of twin embryos formed in the interior of the crystal [57,58]. Defect migration on the twin boundary is driven by local stress tractions on the boundary. These local stresses will most likely be determined by the twin shear and morphology of the embryo, and the deformation reaction of the parent grain, as well as the neighboring grain if the twin embryo is formed at a GB. With these considerations, transition of an embryo into a lamella would depend on embryo shape and orientation of the surrounding crystal(s).

In this work, using microscopy and a 3D crystal plasticity model for discrete twin domains within crystals, we aim to gain insight into the intermediate step of embryo-to-lamella transition. A detailed statistical analysis of the incipient twins in a lightly deformed magnesium polycrystal is performed. They reveal that many wedge-shaped twin embryos lie in the GBs. The calculations are designed to establish the correlation between the local stresses on the crystallographic defects comprising the twin embryo/matrix boundary and the twin embryo-to-lamella transition process. We identify the existence of a critical embryo aspect ratio, that extends over ten times longer in the GB than for self-propagation into the crystal. The analysis further indicates that the stress field induced by the twin would result in a wedge shape. Based on these findings, we rationalize that the wedge-shaped twins in the GB indicate that twin embryos must reach a critical length in the GB to propagate the embryo into the crystal as a wedge shape.

2. Methods

2.1. Experiment

High-purity, fully recrystallized rolled magnesium plate with the strong initial basal texture is used in this work. The initial undeformed microstructure consists of twin-free, equiaxed grains. To activate $\{10\bar{1}2\}$ tensile twinning, the Mg sample was compressed at 10^{-3}/s along the rolling direction. To ensure a sufficient number of early-stage twins in a sufficient number of grains form, the sample was compressed to 1% strain at room temperature. Deformed microstructures were mapped using Electron Back Scatter Diffraction (EBSD) and the collected maps were analyzed using an automated twin analysis software [59,60]. First the deformed material was mechanically ground and polished with 1 μm diamond in propylene glycol and then chemically polished in 10% nitric and water for 10 s. The EBSD data was collected in an FEI XL30 FEG-SEM at 20 kV using a 0.5 μm step size. The reader is referred to [4,5,28,33] for more details about the initial microstructure and texture, mechanical testing, and microstructural mapping and statistical analysis.

2.2. The crystal plasticity model

Twin embryo growth is driven by the stresses acting on the embryo/matrix boundary. Because the embryos lie in a hexagonal close packed crystal, the heterogeneous stresses vary about the embryo and depend on elasticity and crystal plasticity. For this reason, a 3D full-field elasto-visco plastic fast Fourier transform based crystal plasticity (EVP-FFT) model is employed to calculate the local stresses around the twin. This work employs a multi-scale version of this model that builds upon the original infinitesimal EVP-FFT model [61] and incorporates: (1) module for explicit twinning shear transformation simulation [34,62] and (2) dislocation density-based hardening law [63]. For the sake of completeness, the EVPFFT framework, constitutive model, and hardening laws are briefly revisited here.

Under an infinite strain approximation, the elasto-viscoplastic constitutive behavior of the materials is written as,

$$\boldsymbol{\sigma}(\boldsymbol{x}) = \boldsymbol{C}(\boldsymbol{x}) : \boldsymbol{\varepsilon}^{el}(\boldsymbol{x}) = \boldsymbol{C}(\boldsymbol{x}) : \left(\boldsymbol{\varepsilon}(\boldsymbol{x}) - \boldsymbol{\varepsilon}^{pl}(\boldsymbol{x}) - \boldsymbol{\varepsilon}^{tr}(\boldsymbol{x})\right) \quad (1)$$

where $\boldsymbol{\sigma}(x)$, $\boldsymbol{C}(x)$, $\boldsymbol{\varepsilon}^{el}(x)$ are the Cauchy stress tensor, elastic stiffness tensor, and elastic strain at a material point x, respectively. The elastic strain is the difference between total strain $\boldsymbol{\varepsilon}(x)$ and the sum of the plastic strain $\boldsymbol{\varepsilon}^{pl}(x)$ and transformation strain $\boldsymbol{\varepsilon}^{tr}(x)$. Using an implicit time discretization scheme, the Cauchy stress at time $t + \Delta t$ is given by,

$$\begin{aligned}\boldsymbol{\sigma}^{t+\Delta t}(\boldsymbol{x}) = \; & \boldsymbol{C}(\boldsymbol{x}) : \left(\boldsymbol{\varepsilon}^{t+\Delta t}(\boldsymbol{x}) - \boldsymbol{\varepsilon}^{pl,t}(\boldsymbol{x})\right. \\ & \left. -\dot{\boldsymbol{\varepsilon}}^{pl,t+\Delta t}\left(\boldsymbol{x},\ \boldsymbol{\sigma}^{t+\Delta t}\right)\boldsymbol{\Delta t} - \boldsymbol{\varepsilon}^{tr,t}(\boldsymbol{x}) - \boldsymbol{\Delta\varepsilon}^{tr,t+\Delta t}(\boldsymbol{x})\right)\end{aligned} \quad (2)$$

where $\dot{\varepsilon}^{pl}$ is the viscoplastic strain rate. It is assumed to be accommodated by dislocation glide, and thus constitutively related with the stress at material point x through the summation over N active slip systems, of the form:

$$\dot{\boldsymbol{\varepsilon}}^{pl}(\boldsymbol{x}) = \dot{\boldsymbol{\gamma}}_0 \sum_{s=1}^{N} \boldsymbol{m}^s(\boldsymbol{x}) \left| \frac{\boldsymbol{m}^s : \boldsymbol{\sigma}}{\tau_c^s\left(\dot{\boldsymbol{\varepsilon}}, \boldsymbol{T}\right)} \right|^{\boldsymbol{n}} \boldsymbol{sign}\left(\boldsymbol{m}^s : \boldsymbol{\sigma}\right) \quad (3)$$

where τ_c^s is the critical resolved shear stress. A dislocation density-based hardening scheme is used to evolve τ_c^s with strain as a function of the imposed strain rate $\dot{\varepsilon}$ and temperature T. The term $\boldsymbol{m}^s(\boldsymbol{m}^s = 0.5\,(\boldsymbol{b}^s \otimes \boldsymbol{n}^s + \boldsymbol{n}^s \boldsymbol{b}^s))$ is the symmetric part of the Schmid tensor, where $\boldsymbol{b}^s$ and $\boldsymbol{n}^s$ are two orthonormal unit vectors representing the slip direction and slip plane normal, respectively. The shear rate $\dot{\gamma}_0$ is a normalization factor, and n is the rate-sensitivity exponent.

The twin transformation strain within the explicit twin domain is imposed via successive increments using:

$$\boldsymbol{\Delta\varepsilon}^{tr}(\boldsymbol{x}) = \boldsymbol{m}^{tw}\boldsymbol{\Delta\gamma}^{tw}(\boldsymbol{x}) \; = \boldsymbol{m}^{tw}\frac{\boldsymbol{s}^{tw}}{\boldsymbol{N}^{twincr}} \quad (4)$$

where $\boldsymbol{m}^{tw}$ is the Schmid tensor associated with the explicitly simulated twin system, s^{tw} and N^{twincr} are the characteristic twin shear and the number of increments, respectively.

Following the work of [63], the critical resolved shear stress (CRSS) is expressed in terms of dislocation density as:

$$\boldsymbol{\tau}_c^s = \boldsymbol{\tau}_0 + \boldsymbol{b}^s \boldsymbol{\chi} \boldsymbol{\mu} \sqrt{\boldsymbol{\rho}_{for}^s} + \boldsymbol{k}_{deb} \boldsymbol{\mu} \boldsymbol{b}^s \sqrt{\boldsymbol{\rho}_{deb}}\, \boldsymbol{log}\left(\frac{1}{\boldsymbol{b}\sqrt{\boldsymbol{\rho}_{deb}}}\right) \quad (5)$$

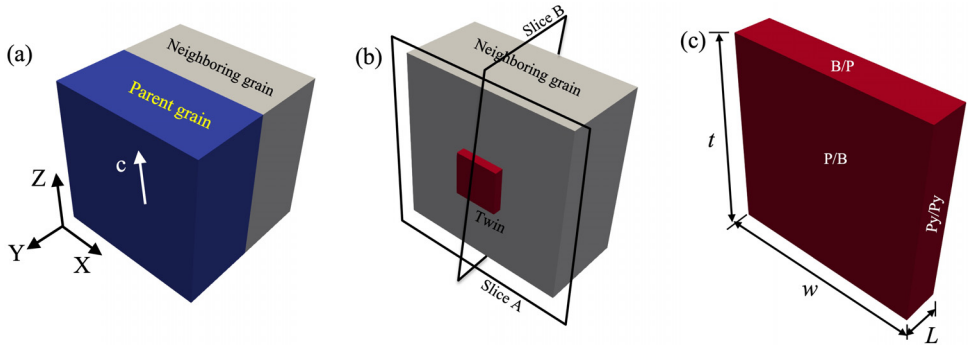

Fig. 2. Geometric and crystallographic details of embryonic twins in Mg grain. (a) Simulation unit cell comprises a parent grain with a 3D twin embryo at the boundary and neighboring grain. (b) Rectangular parallelopiped-shaped twin embryo formed at the GB. (c) The crystallographic details of the twin embryo. Since, the parent grain c-axis is aligned with the Z-axis, the twin embryo boundaries with normal direction aligned with the X-axis, Y-axis, and Z-axis are pyramidal/pyramidal (Py/Py), prismatic/basal (P/B), and basal/prismatic (B/P) facets, respectively. Twin embryo is characterized by its length L, thickness t, and width w.

Here, τ_0 is the initial slip resistance that depends on slip mode, solute density, temperature, and strain rate. The second and third terms represent work hardening due to dislocation-dislocation interactions. In the above equation, the terms χ, μ, k_{deb},ρ_{for}, ρ_{deb} are, respectively, the interaction coefficient, shear modulus, material-independent constant, forest dislocation density and debris dislocation density. The following equation governs the evolution of dislocation density:

$$\frac{\partial \boldsymbol{\rho}}{\partial \boldsymbol{\gamma}} = \frac{\partial \boldsymbol{\rho}_{\boldsymbol{gen}}}{\partial \boldsymbol{\gamma}} - \frac{\partial \boldsymbol{\rho}_{\boldsymbol{deb}}}{\partial \boldsymbol{\gamma}} - \frac{\partial \boldsymbol{\rho}_{\boldsymbol{ann}}}{\partial \boldsymbol{\gamma}} \tag{6}$$

which states that the rate of accumulated dislocation equals the difference between the rate of generation and the rate of removal, which includes the dislocation density that converts to sessile debris, ρ_{deb}, and that is annihilated, ρ_{ann}.

Following the work of Beyerlein et al. [63] for HCP metals, the evolution of dislocation density is expressed as,

$$\frac{\partial \boldsymbol{\rho}^{\boldsymbol{s}}}{\partial \boldsymbol{\gamma}^{\boldsymbol{s}}} = \boldsymbol{k}_1^{\boldsymbol{s}}\sqrt{\boldsymbol{\rho}^{\boldsymbol{s}}} - \boldsymbol{k}_2^{\boldsymbol{s}}\boldsymbol{\rho}^{\boldsymbol{s}} \tag{7}$$

where k_1^s is a coefficient for dislocation storage via statistical trapping of gliding dislocations by forest obstacles and k_2^s is a coefficient for dynamic recovery by thermally activated mechanisms, and it is given as:

$$\frac{\boldsymbol{k}_2^{\boldsymbol{s}}}{\boldsymbol{k}_1^{\boldsymbol{s}}} = \frac{\boldsymbol{\chi}\boldsymbol{b}^{\boldsymbol{s}}}{\boldsymbol{g}^{\boldsymbol{s}}}\left(1 - \frac{\boldsymbol{kT}}{\boldsymbol{D}^{\boldsymbol{s}}\boldsymbol{b}^3}\ln\left(\frac{\dot{\boldsymbol{\varepsilon}}}{\dot{\boldsymbol{\varepsilon}}_0}\right)\right) \tag{8}$$

Here, k, $\dot{\varepsilon}_0$, g^s and D^s are the Boltzmann constant, a reference strain rate, an effective activation enthalpy and a drag stress, respectively. The change in substructure dislocation density is controlled by the rate of recovery of all active dislocations through:

$$\boldsymbol{\Delta\rho_{sub}} = \sum_{\boldsymbol{s}} \boldsymbol{q}^{\boldsymbol{s}}\boldsymbol{b}^{\boldsymbol{s}}\frac{\partial \boldsymbol{\rho}^{\boldsymbol{s}}_{\boldsymbol{rem,for}}}{\partial \boldsymbol{\gamma}^{\boldsymbol{s}}}\left|\boldsymbol{\Delta\gamma}^{\boldsymbol{s}}\right| \tag{9}$$

where q^s is a dislocation recovery rate that quantifies the fraction of dislocations stored as substructure.

The model calculates the equilibrium mechanical fields, such as the strain and stress tensors, everywhere, inside and outside the twin domain, as the crystal by elastic and visco-plastic deformation. The elasticity law used is generally anisotropic with five elastic constants for a hexagonal close packed material. For Mg, we use experimentally measured constants at room temperature which are: $C_{11} = 59.5$; $C_{12} = 26.1$; $C_{13} = 21.8$; $C_{33} = 65.6$ and $C_{44} = 16.3$ in GPa [64], which we note corresponds to a nearly isotropic material. Plastic deformation follows crystal plasticity theory, permitting deformation via basal $\langle a \rangle$, prismatic $\langle a \rangle$, and pyramidal $\langle c + a \rangle$ slip modes. The initial CRSS and the associated hardening parameters for these slip modes used in the dislocation density hardening model Eqs. (5)-(6) are taken from [65].

2.3. Model setup

Fig. 2(a) shows a schematic of the 3D bi-crystal simulation unit cell comprising a parent grain with a twin embryo and the neighboring grain. A buffer layer with uniformly distributed crystal orientation surrounds the entire bi-crystal, not shown in Fig. 2. The crystallographic orientation of the parent grain in the Bunge convention is $(0^o, 0^o, 0^o)$. It aligns the c-axis of the parent grain with the Z-axis of the unit cell. The neighboring grain crystallographic orientation is chosen differently for different cases to demonstrate the effect of neighbors on the local stresses associated with twin embryos. A set of voxels in the parent grain at the grain boundary (GB) is preselected as the twin embryo. An isolated view of the twin at the GB is shown in Fig. 2(b).

Twin embryos are three-dimensional domains that formed most often at the GBs [4-6,66]. Commonly the 3D twin domain boundaries are associated with twin crystallographic directions such as the twin plane normal, twin shear direction (commonly referred as forward direction) and lateral propagation/growth direction [49,50,56,67-71]. The normal twin boundary is composed mainly of a coherent twin boundary (CTB) along with a few P/B and B/P facets [49,67-69]. Here P/B facet refer to a twin interface where in which the prismatic plane of twin is parallel to the basal plane of par-

ent crystal, and vice versa for B/P facets. The twin forward boundaries form because of edge-type twinning dislocations and mainly contains B/P and P/B facets [50,56,70,71]. The lateral twin boundary is reported to form by screw type twinning dislocations and contain pyramidal/pyramidal (Py/Py) and prismatic/prismatic facets [49,67,68]. The earlier two-dimensional atomistic studies suggest that the twin embryos are composed of P/B and B/P facets and their growth will form the CTBs [23,72,73]. Following these works, here, the 3D twin embryo is assumed to be surrounded by P/B, B/P and Py/Py facets. Since, the c-axis of the parent grain is aligned with the Z-direction of the simulation cell, the normal vector to the P/B, B/P and Py/Py facets are parallel to the Y, Z and X directions, respectively, see Fig. 2(c).

The twin embryo is characterized by its length (L) into the crystal and its thickness (t) and width (w) within the GB plane. The twin propagation conventionally refers to increases in L and thickening usually to increases in t and/or w. Three-dimensional experimental characterization of the twin embryo is needed to appropriately choose the shape and sizes. But most of the experimental literature and the present work is two dimensional as surfaces are analyzed. Further, In turn, it is nearly impossible to obtain the three-dimensional morphology of the twin embryo. Thus, for the sake of simplicity, in the work, the initial twin embryo thickness (t) and the width (w) are assumed to be the same (see Fig. 2). This will be suitable in identifying a critical value of the ratio t/L. In most standard crystal plasticity calculations, individual dislocation lines are not explicitly modeled. Thus, material points in such calculations most appropriately apply to distances between material points that are more one to two orders of magnitude than the core of a dislocation (~0.5 nm). Thus, twin embryos that are at least 50 to 100 nm in one dimension can be modeled, which aligns well below the sizes of embryos seen experimentally [9,66,74].

3. Results and discussion

3.1. Twin thickness t at GBs

Fig. 3 displays a representative EBSD image of the pure Mg sample after compression. Despite being lightly deformed, extensive activation of tensile twins is evident and most of twin lamellae fully span the grain and contact another GB. However, twins that terminate inside the crystal are also seen. We refer to these terminating twins as *early-stage twins* as they are undergoing the embryo-to-lamella transition, and are clearly not embryos nor are they advanced twin lamellae. Most importantly, most early-stage twins have a wedge shape, where the thickness of the twin overlapping the GB is thicker than that of the tip that terminates in the crystal. Some early-stage twins are connected at the same location in the GB to another twin in the neighboring grain and are referred to here as *connected twins*. Other early-stage twins at GB have no direct connection with any other twin and are referred as *isolated twins*. Both the isolated and connected twins are marked in Fig. 3.

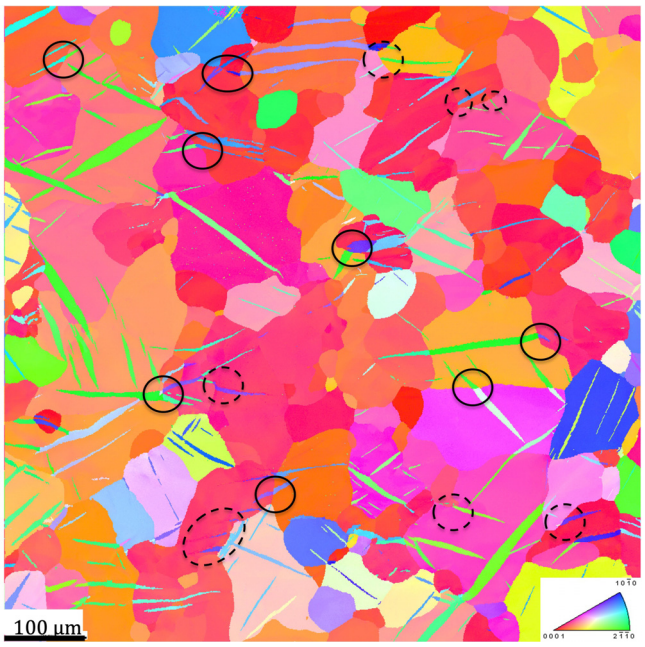

Fig. 3. EBSD image showing several early-stage $\{10\bar{1}2\}$ tensile twins in high pure Mg exhibits wedge shape. A few of these twins are indicated by a black circle. The concept of wedge shape twins is true for both isolated (dashed line) and connected twins (solid line).

Terminating twins, as well as their wedge shape, are not often discussed or reported. Closer inspection of previously published EBSD data on a deformed Mg alloy reveals similar wedge-shaped GB twin embryos [48]. Fig. 1(b) shows a few twins in their early stages of growth, in which they have already propagated into the crystal but terminated inside the matrix grain taken from [48]. Here the $\{10\bar{1}2\}$ tensile twin is activated in an Mg-Gd-Y-Ag-Zr alloy. The wedge-like shape of these twins is apparent with a broader base lying in the GB and the finer tip of the wedge protruding into the crystal. Inspection of EBSD micrographs from a study focused on incipient $\{1012\}$ twins in Ti similarly reveals many submicron-sized wedge-shaped twins terminating in the interior of the grains. Note that this observation of the wedge shape of these twins is not discussed in these works.

The submicron scale thickness at the GB of these early-stage twins suggests that each one originated in the GB and before it could propagate across the entire crystal, it grew into the observed wedge shape. How the embryo transitioned from a seed lying within the GB to a wedge-shaped early-stage twin is unclear. Using 3D discrete twin crystal plasticity techniques, many studies have shown that the stress field ahead of a twin with uniform thickness is sufficiently high to support its propagation, but not its thickening [34,62,75,76]. Such predictions of self-propelling twin-tip stress fields have been supported by experimental evidence. [40,44,77-79]. Thus, it is unlikely that the wedge shape of early-stage twins was formed by the twin first propagating into the crystal followed by thickening at the GB. Accordingly, the converse is the more likely scenario. The embryo had to first expand within the GB to a critical thickness before propagation into the crys-

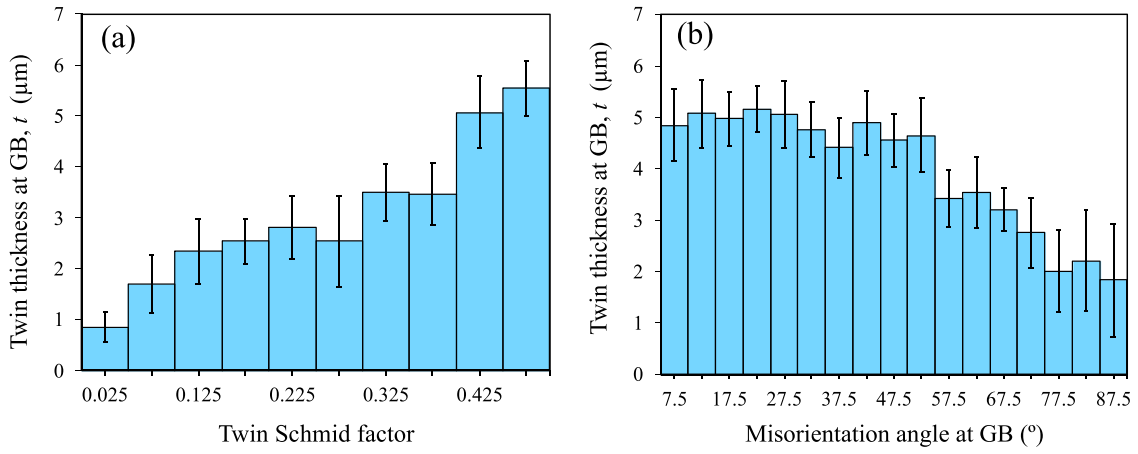

Fig. 4. Statistical analysis of twin thickness at GBs (t). Distributions of twin thickness at the GB as a function of (a) twin Schmid factor and (b) GB misorientation angle.

tal is favorable. Much like it has been proposed that interior ellipsoidal embryos need to grow to a certain characteristic major-to-minor axis ratio before expanding into a lamella, GB embryos may also need to expand to a certain thickness within the GB before propagating away from the GB into the parent crystal.

Twinning is well known to be a statistical event, and thus to obtain quantitative confirmation of the wedge shape of early-stage twins, a detailed statistical analysis is performed. Several EBSD maps of lightly compressed Mg were collected, and the maps were analyzed using an automated twin analysis software [59,60]. The number of grains, twins and GBs investigated in this work respectively are: 1254, 4875 and 18,542. Among 4875 twins, only 318 early-stage isolated twins are considered for statistical analysis.

Analysis of these 318 twins confirms a prevailing wedge shape of early-stage twins. Fig. 4(a) plots the thickness of the twins within the GB t as a function of the twin Schmid factor, which is a projection of the twin plane and the twin direction with respect to the applied load. It would be expected that if twins were stress-driven then t would increase with its Schmid factor. The data show that this is indeed the case. The remarkable finding is that a minimum thickness t_{min} appears even for twins that formed with nearly zero Schmid factor. Apart from the Schmid factor, it is commonly reported that the neighboring grain orientation can significantly influence the twin thickness that overlaps with GB [62,75,76,80]. Fig. 4(b) shows the correlation between the GB twin thickness t and the (minimum) misorientation angle between the grains. Here, the t decreases with increasing misorientation angle. A similar trend has been reported in previous studies, where they found that twin thicknesses at the GB from where the twin originated were thicker than that at twin/boundary junctions where they terminated [4,80]. In addition, the distribution in Fig. 4(b) clearly implies a strong influence of the neighboring grain orientation, a point we return to later. We should note that since these are 2D cross sections of 3D twins, the twin thickness is not the thickness of the actual twin in the absolute sense. Nevertheless, it is clear that these early-stage twins bear a wedge shape and that even when considering the full range of parent or neighboring grain orientations, including those that would not favor or be suitable for twinning, a minimum GB t_{min} still exists. Further, it is orders of magnitude higher than any theoretical or numerically predicted stable twin embryo size. This supports the concept of a critical GB thickness for twin propagation; the GB embryo had to first expand within the GB before propagating into crystal.

3.2. Stress fields on faceted twin embryo boundaries

Twin embryos and twin lamellae alike expand their volume by migrating the twin/matrix boundary. At the length scale studied, the crystallography of the matrix and twin domains and twin boundary surface dictate the local stress and strain fields. Due to the twin shear alone, these boundary tractions can grow sufficiently intense to invoke localized plastic deformation at the boundary and in the vicinity of the embryo. In this section, the stress state produced by a model 3D embryonic twin (Fig. 2) is calculated via the full-field, spatially resolved crystal plasticity technique EVP-FFT and analyzed to determine whether the nature of the stress (directionality, sign, magnitude) is sufficient to migrate any portions of the embryo/parent boundary.

The simulation begins with an already formed elementary 3D embryo (see Fig. 2), the smallest unit seed from which forward, lateral, and transverse expansion is possible, and under a pre-assigned applied stress. The latter is imposed because it is very likely that such embryonic seeds would have formed under mechanical stress. Prior work finds that the variant of the twin embryo corresponds to one with the highest twin resolved shear stress (TRSS) from the local stress state [4,6,28]. To best represent these conditions, a far field mechanical loading is first applied to the outer polycrystal, when the material is twin-free. In the present calculations, a far-field compressive strain of 0.5% in the Y-direction is applied since it is presumed sufficient to induce a local stress in the parent grain that would form a {1012} twin embryo. Next, while under fixed macroscopic strain, the twin embryo is formed in the

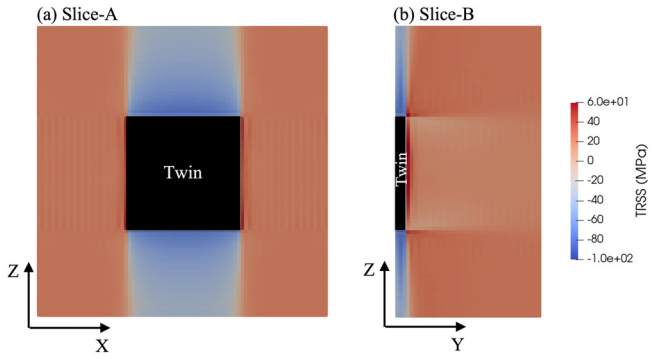

Fig. 5. Model calculated twin plane resolved shear stress (TRSS) field after the formation of the twin embryo (a) in slice-A, which is adjacent to the GB in the parent grain and (b) in slice-B, which shows the cross-section of the twin embryo. Refer Fig. 2(b) for details of slice-A and B. Here, size of the twin embryo is: $L = 3$, $t/L = 7$ and $w/L = 7$.

preselected domain by reorienting the lattice according to the twin/matrix relationship and imposing the characteristic twin shear. In all the stages, the deformation is accommodated by anisotropic elasticity and visco-plasticity as mediated by crystallographic slip.

From the model calculated full stress tensor, the twin plane resolved shear stress (TRSS), which is commonly considered as a driving stress for twin nucleation and growth, is calculated. Fig. 5 shows the TRSS distribution in two cross-sections, slices-A and -B, after the formation of a twin embryo. The twin domain is the black region. Here the neighboring grain orientation is the same as the parent grain to eliminate neighbor effects. Slice-A in Fig. 5 is parallel to the X-Z plane and taken at a point in the parent grain next to the GB, see Fig. 2(b). This slice provides the distribution of micromechanical fields at the B/P and Py/Py facet interfaces. Slice-B, which is parallel to the Y-Z plane, reveals the fields at the P/B and B/P facets. The TRSS distribution in slice-A shows that expansion of embryo by migrating the Py/Py facet is favorable, but not so by the P/B facet. This observation suggests that lateral growth of the twin is favored over thickening, which is in agreement with prior reports [26,81,82]. Fig. 5(b) shows the TRSS field in slice B. It reveals that the local stress at the P/B facet face favors its migration. Slice-A helps to understand the possibility of expanding twin domain along the GB, whereas slice-B provides information on forward migration of the twin tip into the crystal. To understand the embryo-to-lamella transition by the propagation of twin tip into the crystal, only slice-B is considered hereafter.

Although the TRSS is commonly used as a driving force for twin formation, the crystallographies of these three twin facets indicate that the stress traction that would drive their migration are not necessarily the same. Fig. 6(a) shows the crystallographic plane arrangements of the P/B, B/P and CTBs when the c-axis of the parent grain is parallel to the Z-axis. The boundary B/Ps and P/Bs lie parallel to the Y-axis and Z-axis, respectively, and the CTB lies on the {1012} plane. For CTB migration, a positive TRSS shear stress is needed. For Mg, the separation between the basal planes is 5.21 A^o and the prismatic planes is 5.55 A^o. Accordingly, to migrate a B/P facet, a tensile traction acting on the B/P face is needed, and likewise, to migrate a P/Bs facet, a compressive traction on its face is required. The stress components that drive migration for each facet are schematically shown in Fig. 6(b).

Fig. 6(c) shows the calculated driving force, the S_{YY} component, for migrating the P/B facet along the facet face of the model embryo. At the twin front, the S_{YY} is compressive, ranging from ~ -24 MPa to ~ -7 MPa, with the highest compressive (minimum S_{YY}) value generated in the center of the facet. The sign and profile of S_{YY} across the facet suggest that the migration of P/B facet into the crystal would be favored and more importantly would develop into a wedge shape. Whether the magnitude of these compressive tractions can propagate the twin depends on local material strengths. The significant finding is that tractions on the P/B facets of an embryo have the sign and character needed to grow the embryo into the crystal. Since these features result predominantly from the interaction of the twin shear of the embryo itself and the surrounding matrix, the embryo could self-propagate should the intensity of S_{YY} reach a characteristic material strength.

3.3. Critical aspect ratio for twin embryo expansion

The aforementioned calculation considers only one embryo aspect ratio of $t/L = 7$, for which S_{YY} had the sign and character needed for propagation. Whether these self-propelling stresses meet this criterion would depend on t/L. To identify this dependency, we repeat the calculations for aspect ratios (t/L) ranging from 1 to 21. The t/L values of interest are greater than unity since the notion tested is that the embryo needs to grow in the plane of the GB before it can propagate away from it.

Fig. 7 shows the S_{YY} stress field along the P/B front for the full range of $t/L \geq 3$. Only for $t/L > 5$, the S_{YY} values are compressive. P/B migration is, therefore, possible as along as the embryo is extended within the GB more than 5 times its length out of the GB plane (see Fig. 6(b)). Also, for all t/L, the S_{YY} profile is nearly symmetric, minimizing at the center of the P/B front. The variation arises due to the reaction of the surrounding crystal to the twin shear at the two ends of the embryo. The distribution of TRSS along twin front (see Fig. 5) also peaks at the center and decreases gradually to the edges. Overall, these stress profiles in the twin embryo front face suggest that the region most likely to first propagate is the center of the embryo front.

The migration of the B/P facets on the lateral sides of the embryo requires the driving stress S_{ZZ} to be tensile. Calculations find that the S_{ZZ} ranges from -150 to -170 MPa for the full range of t/L (not shown). Lateral migration of the B/P facets for thickening the embryo within the GB is not possible when $t/L > 1$. This means that for the same t/L range that the P/B facet can migrate away from the twin, the B/P facets cannot migrate.

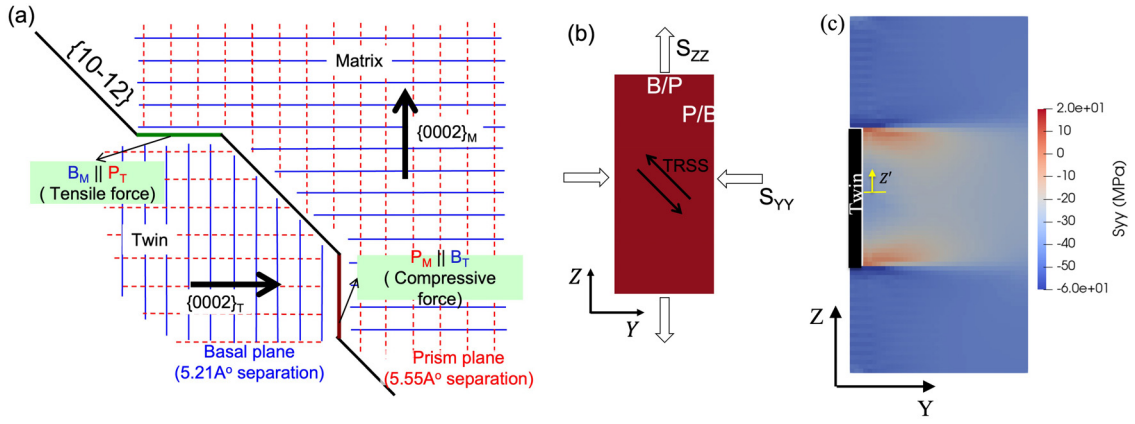

Fig. 6. (a) The crystallographic details of twin interfaces P/B, B/P and CTBs. (b) Based on the crystallographic plane separation, the favorable stress required for the migration of P/B and B/P facets are compressive (S_{YY}) and tensile (S_{ZZ}) stresses, respectively. (c) The model calculated S_{YY} distribution at the twin front (slice-B) for an embryo of L= 3, t/L = 7 and w/L = 7.

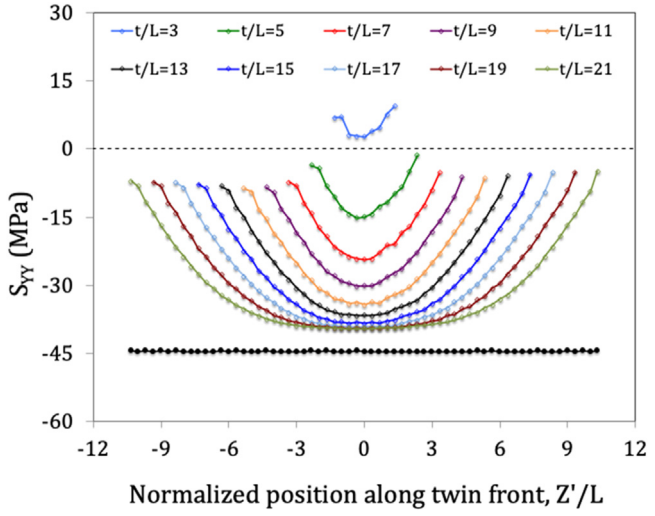

Fig. 7. Distribution of S_{YY} along twin front for different twin thicknesses (t/L) from 3 to 21. The stress profiles before the formation of twin also shown in black. Here the twin length is fixed as L = 3. Increase in the twin embryo thickness in the GB plane increases the twin driving stresses and it saturate for higher t/L.

The TRSS distribution across the Py/Py facet shown in Fig. 5 suggests that the twin embryo can expand in the GB plane in its width (w) dimension. In the calculations thus far, $w = t$. Thus, this poses a natural question of whether a twin embryo can propagate into the crystal even for smaller t/L, while w/L is larger. To address this, calculations were performed for the full range of w/L with $w/L \geq t/L$ and fixed t/L = 3 or 7. For both t/L, the S_{YY} profiles shown in Fig. 7 do not change significantly (sign and magnitude) for varying w/L. It confirms that w/L of the embryo in the GB plane is not governing the migration of the P/B facet into the crystal. Thus, in the rest of the analysis, the w/L is assumed to be the same as t/L.

The results identify that the "self-stress" induced by the twin embryo alone is directed to extending it into the crystal but not thickening it within the GB. In addition, if a constant critical force criterion is applied to the twin front, it will likely start to migrate heterogeneously, starting in the middle. It can be easily anticipated that a wedge-like twin front would form as a result. Another important finding made here is that the P/B migration stress S_{YY} is more likely to reduce (become more compressive) and favor propagation into the crystal as t/L of the embryo increases. More significantly, the minimum value of S_{YY} across the facet lowers as t/L increases until at some critical $(t/L)_c$, and it reaches a saturation point, as shown in Fig. 7. To identify $(t/L)_c$, we first identify the minimum S_{YY} for each t/L, over a much broader range from 1 to 30. Fig. 8 clearly suggests that $(S_{YY})_{min}$ drops with t/L, becoming compressive once $t/L > 3$, and it saturates at some critical $(t/L)_c$ that lies $t/L > 14$. To estimate $(t/L)_c$, the percentage of change in $(S_{YY})_{min}$ for a change in t/L is calculated and plotted versus the secondary, right-hand axis in Fig. 8. The change becomes almost negligible (here we choose 1%) when $(t/L)_c = 16$ as marked in Fig. 8.

The significance of these results is that they reveal the existence of critical $t/L >> 1$ for self-propelled embryo-to-lamella transition. Again, we mention that when given a characteristic critical force needed to extend the twin, a critical twin embryo shape and size can be determined.

3.4. Grain neighbors that promote expansion

Atomic scale calculations and analytical models for twin nucleation have suggested that embryos that originate at GBs may have to grow within and along the GBs before extending into the crystal [23,72,83]. The calculations performed here indicate that the stress field along its boundaries generated by the characteristic twin shear within the 3D embryo domain introduces an unanticipated t/L effect for embryo propagation. To focus on t/L effects, the neighboring grain orientation was set to be the same as the parent grain orientation. This scenario can be considered as the nucleation of twin embryos inside the grain. The simulation results suggest that the lo-

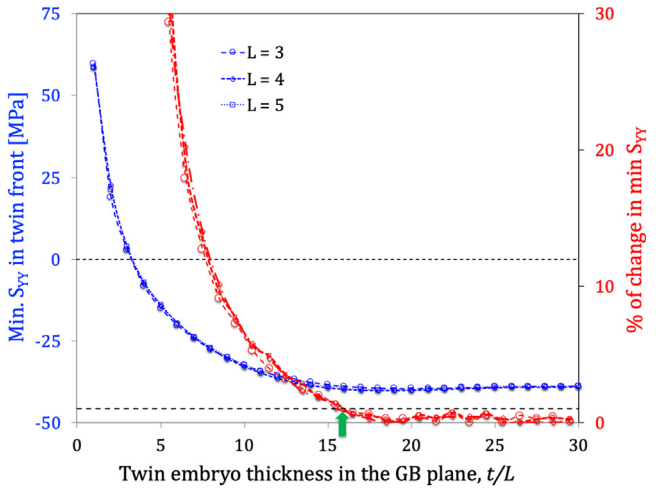

Fig. 8. Concept of critical twin thickness in the GB plane. Distribution of maximum twin embryo driving stress at the embryo P/B facet as a function of *t/L*. The twin driving stress increases with embryo *t/L* and saturate after critical *t/L*. The change in twin driving stress for increase in twin *t/L* is also plotted in the secondary vertical axis. Here different twin length cases ($L = 3$, 4 and 5) also shown and it confirms that the predicted optimal twin AR is insensitive to simulation size. The selected minimum change in stress (here 1%) for the identification of critical twin embryo thickness (marked by green arrow) is shown by a dashed line.

cal stresses favor the propagation of the twin embryo, and it can eventually reach the grain boundaries. However, it is commonly reported that the deformation twins mostly nucleate at the grain boundaries where local stress concentration and defects are present. In this usual scenario, the neighboring grain orientation differs from the parent. Since the neighboring grain is another Mg crystal, which is known to have a highly plastically anisotropic response, it can be expected that the embryo-boundary stress fields could depend on the orientation of the neighbor and its ability to dissipate the strain energy caused by the twin shear. To study this aspect, the calculations are repeated for the total of 221 neighboring grain orientations for the same fixed parent grain orientation. For each orientation $(S_{YY})_{min}$ is obtained for a range of *t/L* from 1 to 30. Using the same procedure as in Fig. 8, the $(t/L)_c$ is identified.

Fig. 9(a) presents the distribution of $(t/L)_c$ for all neighboring orientations. In this analysis, the neighboring grains are classified by a factor that measures their ability to plastically accommodate the twin shear imposed by the embryo. In this regard, in prior works, the relative position of a given slip mode in the neighboring grain with respect to the twin has been considered an appropriate factor to classify the neighboring grain orientation [33,75,84]. This factor is given by,

$$\boldsymbol{m'} = (\boldsymbol{b_T}.\boldsymbol{b_s})(\boldsymbol{n_T}.\boldsymbol{n_s}) \tag{7}$$

where, $\boldsymbol{b}_T$ and $\boldsymbol{n}_T$ is the Burgers vector and plane normal of the simulated twin system in the parent grain, and $\boldsymbol{b}_s$ and $\boldsymbol{n}_s$ is the Burgers vector and plane normal of different slip modes of the neighboring grain. If the value of m' is 1.0, then the shear imposed by the twin variant in the parent is well aligned to cause shear on this particular slip system in the neighbor. Using this measure, a plastically soft neighbor would be oriented such that m' is not only non-zero on many slip systems, but predominantly on the ones that are relatively easier to activate. Likewise, a plastically hard neighbor may have a non-zero m' on slip systems that are harder to activate. Since the easiest slip mode is basal $\langle a \rangle$ slip in Mg, only the m' of basal slip mode is considered in Fig. 9(a) [75].

Fig. 9(a) reveals that $(t/L)_c$ decreases with increasing m'. The neighboring grain that is better suited for accommodating the embryo twin shear via basal slip, the more easily the embryo-to-lamella transition occurs or equivalently, the smaller the $(t/L)_c$ (i.e., smaller the embryo GB thickness needs to be).

For comparison, Fig. 9(b) shows the experimentally measured GB thickness of the isolated early-stage twins observed in the deformed Mg as a function of the relative orientation of the basal slip (m'). Here, the maximum m' among all three basal slip systems and the early-stage twin variant is used in this analysis. Fig. 9(b) clearly reveals that the twin thickness at the GB decreases with an increase in the relative position of basal slip in the neighboring grain.

3.5. Wedge shape twin embryo propagation

The twin front stress profiles shown in Fig. 7 suggest that the propagation of the embryo may follow a wedge shape. To test whether the wedge-like step formation at the embryo front favors further propagation and growth, here, a quasi-dynamic step-by-step twin propagation simulation is performed. First, a twin embryo of size $\frac{t}{L} = \frac{w}{L} = 7$ and $L = 3$ is introduced. The stress field at the front of this initial twin embryo favors propagation, see Fig. 7. Based on this stress profile, a domain is identified for formation of a smaller twin step (or protrusion). The dimension of the protruded twin domain is chosen to be $\frac{t_{step}}{L_{step}} = \frac{w_{step}}{L_{step}} = 5$ and $L_{step} = 1$. This leads to a wedge-like twin morphology. This protruded twin is formed by lattice reorientation and imposing twinning shear strain. The TRSS profile along the protruded twin front and adjacent to the GB are plotted in red in Figs. 10(a) and (b), respectively. For comparison, the TRSS profiles after the formation of initial twin embryo are also shown in blue. Fig. 10(a) reveals that the TRSS profile at the twin front increases when the wedge-like twin propagation has performed. Thus, twin propagation propensity increases even further when the wedge shape has formed. Similarly, the TRSS profile along the GB shown in Fig. 10(b) suggests that the wedge-shape twin propagation increases the local stresses around the twin, and that favor the thickening process. Overall, the simulations results support the proposed wedge-like propagation of twin embryo into the grain.

3.6. Remarks on sensitivity to model conditions

Before continuing further, it is worth remarking on the sensitivity of the findings to some of the preset model conditions.

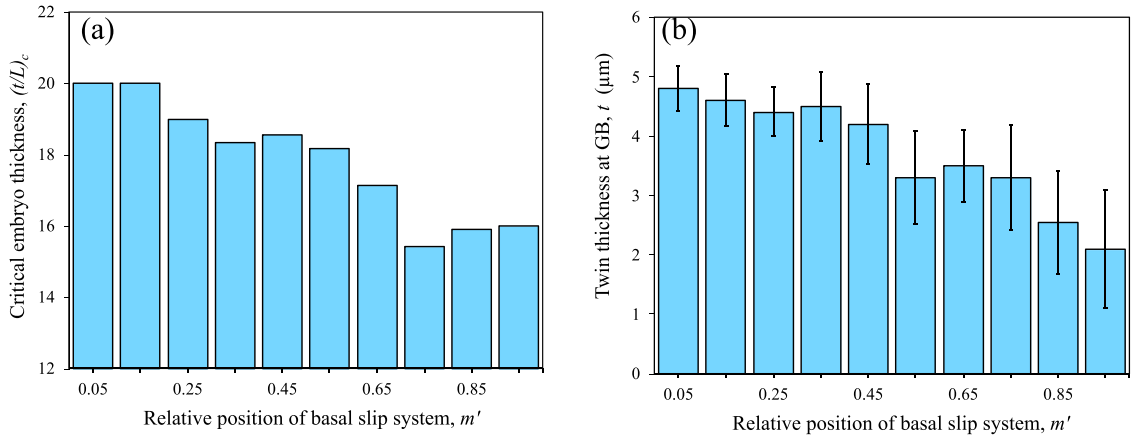

Fig. 9. Distribution of (a) model predicted critical twin embryo thickness $(t/L)_c$, and (b) experimentally measured twin thickness at GB (t) as a function of relative position of neighboring grain basal slip mode with respect to the simulated/activated twin (m′).

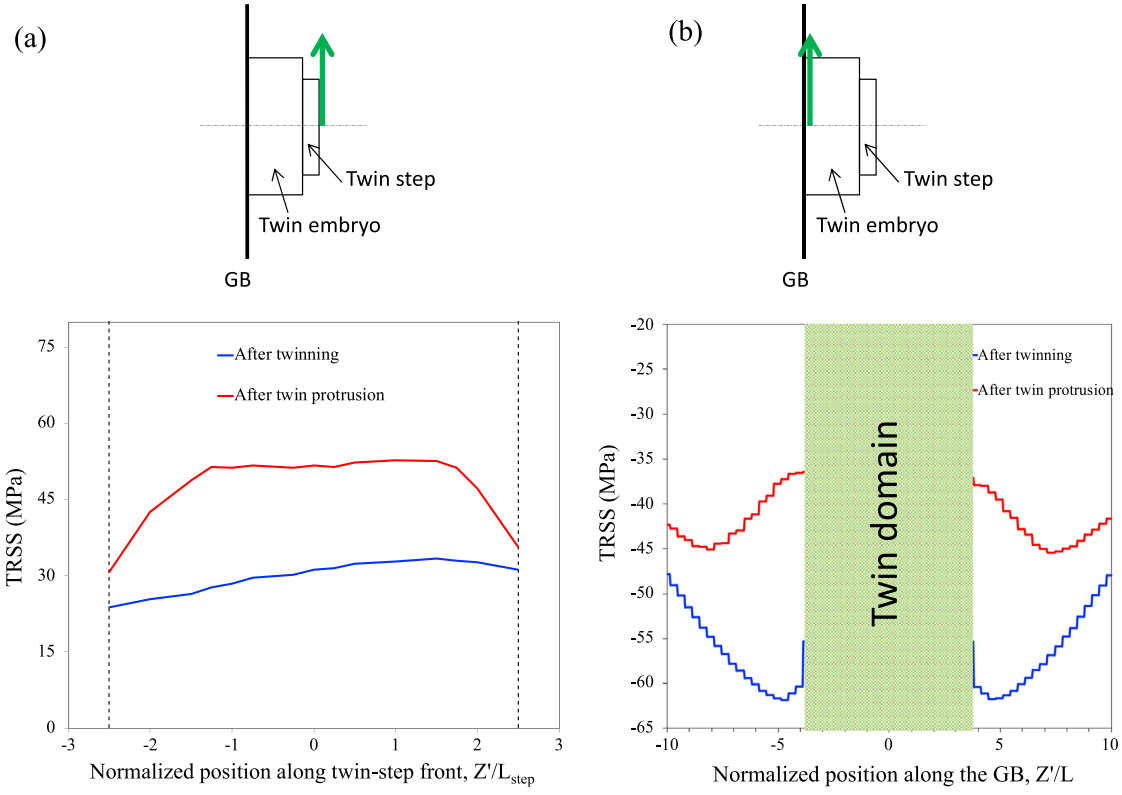

Fig. 10. Distribution of TRSS along (a) twin front and (b) adjacent to the GB for wedge shape propagation case. The stresses after the formation of initial twinning and after the twin-step formation are plotted in blue and red, respectively. Here, the geometry of the initial twin embryo: $\frac{t}{L} = \frac{w}{L} = 7$ and $L = 3$, whereas the geometry of the twin step: $\frac{t_{step}}{L_{step}} = \frac{w_{step}}{L_{step}} = 5$ and $L_{step} = 1$.

The calculations discussed thus far were carried out in a particular applied loading direction. In actuality, the loading/grain orientation relationship can vary. The findings reported here originate from the self-stress created by the twin embryo and arise due to a coupling between the twin shear and the elastic and plastic response of the surrounding crystal(s). Therefore, an overpowering effect of external loading is not anticipated. At the same time, based on our previous studies, it is expected that compared to the external stress, the local stress may play a more dominant role in the reported critical embryo thickness for propagation. Further, the variations in t/L were accomplished by changing the thickness while keeping the length constant. With the model, it is just as possible to change the length instead to achieve the same t/L. We repeated the calculations for various L ranging from 3 to 5, and the results are also shown in Fig. 8. It is clear that the results de-

pend on *t*/*L*, not *L* alone independently. Furthermore, as stated in Section 2.3, since the actual three-dimensional morphology of the embryo is not known, the thickness and width of the modeled twin embryo are assumed to be the same. Despite of the same size, the simulation result shown in Fig. 5 indicates that the TRSS fields are significantly different in the thickness and width direction. Thus, one can speculate that the embryo thickness and width cannot be the same.

3.7. Mechanisms for embryo thickening

This study introduces a new concept of a critical $t/L >> 1$ for a GB embryo, above which self-propelled propagation is possible. The physical picture this criterion paints is that the embryo is an order of magnitude thicker in the plane of the GB than normal to it. However, twin embryos, when they first form in the GB are nm in dimension, have low aspect ratios, and are detectable only via TEM or HR-TEM. These seedling embryos, thus, possess subcritical thicknesses, possibly explaining why they are not seen to propagate into the crystal. In fact, many embryos could form at the GB under the appropriate defect and stress conditions [23,72]. They may even be stable, that is, they would not shrink or detwin when the external load is released. Yet still, the existence of a critical thickness implies that even stable embryos cannot propagate into the crystal and move across the crystal by forming a lamella unless they have grown to a sufficient thickness within the GB. It would explain the minimum GB twin thickness seen here in the statistical analysis of hundreds of early-stage twins.

Twin embryos when they first form are likely of subcritical *t*/*L*. The question that remains is how an embryo can achieve a sufficiently high aspect ratio ($\frac{t}{L}$). Analysis of the boundary stresses on the B/P facets indicate that boundary stresses act against thickening. An alternative mechanism to stress-driven B/P migration is needed for thickening. One reasonable proposal is that the thicker embryo is constructed by the nucleation of several, closely spaced smaller, subcritical twin embryos or so-called "seeds". Prior work on parallel twin lamellae has shown that when closely spaced, by distances ranging from a few to several times their thickness, the back-stress on the boundary that resists widening increases beyond that generated by an isolated twin [62]. Thus, the formation of a thicker embryo by the coalescence of smaller twins is not a plausible mechanism. It suggests that atomic descriptions would be necessary to understand the development of a super embryo. In Wang et al. [23,72] atomistic simulations of twin formation at HCP symmetric tilt boundaries showed that multiple tiny (∼nm) twin seeds form at GB defects when acted upon by an impinging pile-up. As more seeds formed along the GB and became closely spaced, they appeared to eventually merge, producing a single embryo several tens of nm thick along GB. While the atomic-scale process was not detailed, it seems that more seeds formed both in between and outside the first seeds. As more support, a recent in-situ experimental study on Mg observed the development of a wide twin embryo in a defective boundary via the nucleation of several closely spaced twin seeds [66,74]. Thus, for embryos to reach the needed thickness in a GB, the GB would need to be sufficiently defective such that under stress create multiple, closely spaced twin seeds that together span a region several tens of nm in size. The spacing between the tiny twin seeds should be small enough that the elastic/plastic strain field interactions between them may not play a role in their merger.

The calculations show that the driving force to push out a twin embryo increases as the twin becomes thicker. While thicker twins can propagate easily, the twin cannot thicken by its own self-stress. This dilemma may explain why twins in HCP metals generally do not form easily and are a rare statistical event. The size effect or critical "thickness" revealed here suggests that while many stable GB embryos could form, only some can propagate away from the GB. This may explain why twins seen to start to propagate have a minimum thickness at the GB from which they originate. The strong grain neighborhood effect on the critical thickness seen here would imply that some neighboring grain orientations can favor twinning, while others do not, and thus, the same suitably oriented parent grains in the polycrystal would not all equally support twin propagation.

3.8. Impact on the design of high-performance materials

The findings here can substantially increase the amount of information gained from microscopy analyses of deformed Mg alloys. To quantify microstructure-twin relationships and gain an understanding of deformation twinning, orientation mapping of deformed materials is being continuously being pursued, and to date, these have been advanced to include automated acquisition of statistically significantly large data sets (several thousands of twins) in 2D and even 3D [4-6,26,28,80,85]. Apart from carrying out in-situ deformation studies, the findings here indicate where twins originate and where they terminate. Our results imply that twins will be relatively thick at their GB of origin and relatively thin at GBs they intersect. Further, twins that terminate inside the crystal, having not yet propagated across the grain, will have a wedge shape with their thick wedge base along the GB, where they originate. The thickness of the twin where it overlaps the boundary will likely correspond to the thickness of its critical shape.

These findings also suggest significant changes need to be made in the way higher-length scale models treat twinning. Many constitutive laws involved in the development and design of structural HCP metals have reached a level of sophistication that they can account for the formation and growth of twin lamella inside grains and their interaction with crystallographic slip in the calculations of texture evolution and stress-strain response [86–90]. These models, however, require criteria for the formation and growth of these twins, since they are based on processes operating at length and time scales much below those accessible by the model. At present, they predict well the thickness of twin variants that are well oriented with respect to the applied loading, so-called "high-Schmid factor

twins", but grossly underestimate by 200% the thickness of observed low Schmid factor twins [65,75]. The former is suitably oriented to continue thickening beyond the thickness of its critical embryo, but the latter is likely to not grow further and hence preserve its original critical width.

4. Conclusions

In this work, the transition of twin embryo to sub-micron scale lamella is studied using the experimental and numerical methods. Detailed statistical analysis of early-stage twins in the deformed Mg microstructure is performed to establish the correlation between the twin thickness at the grain boundaries, and the misorientation angle and the relative position of easy slip in the neighboring grain. A full-field, spatially resolved crystal plasticity model, called elastic-visco-plastic fast Fourier transform (EVPFFT), coupled with a dislocation density-based hardening model, is employed to quantify the local stresses at the interfaces that borders the twin embryo. This combined experimental and computational study leads to the following key findings.

1. Experimental statistical analysis shows that the thickness within the grain boundary (GB) of early-stage twins decreases with increasing misorientation angle and increasing misalignment between the twin embryo variant and basal slip in the neighboring grain.
2. The twin embryo formed in a GB can propagate if its thickness at the GB (t) is significantly larger than the length of the embryo (L) into the crystal, $t/L >> 1$.
3. The local driving stress profile along the twin front indicates that propagation initiates in the center of the facet and, thus, is most likely to develop into a wedge shape with a thick base at the GB.
4. The model calculations show that the more aligned the twin variant is with basal slip in the neighboring grain (greater m'), the smaller the critical aspect ratio needed for propagation.

Data availability statement

Data available on request from the authors: The data that support the findings of this study are available from the corresponding author upon reasonable request.

Declaration of competing interest

The authors declare that they have no known competing financial interests or personal relationships that could have appeared to influence the work reported in this paper.

Acknowledgments

This work is funded by the U.S. Dept. of Energy, Office of Basic Energy Sciences Project FWP 06SCPE401. IJB acknowledges support by the National Science Foundation under Grant Number 2051390.

References

[1] P.G. Partridge, Metallur. Rev. 12 (1967) 169–194.
[2] M.H. Yoo, Metallur. Trans. a-Phys. Metallur. Mater. Sci. 12 (3) (1981) 409–418.
[3] M.H. Yoo, J.K. Lee, Philosoph. Mag. a-Phys. Condens. Matter Struct. Defects Mech. Properties 63 (5) (1991) 987–1000.
[4] I.J. Beyerlein, L. Capolungo, P.E. Marshall, R.J. McCabe, C.N. Tome, Philos. Mag. 90 (30) (2010) 4073–4074.
[5] L. Capolungo, P.E. Marshall, R.J. McCabe, I.J. Beyerlein, C.N. Tome, Acta Mater. 57 (20) (2009) 6047–6056.
[6] M.A. Kumar, M. Wroński, R.J. McCabe, L. Capolungo, K. Wierzbanowski, C.N. Tomé, Acta Mater. 148 (2018) 123–132.
[7] R.J. McCabe, G. Proust, E.K. Cerreta, A. Misra, Int. J. Plast. 25 (3) (2009) 454–472.
[8] B.M. Morrow, R.J. McCabe, E.K. Cerreta, C.N. Tome, Mater. Sci. Eng. a-Struct. Mater. Properties Microstruct. Process. 574 (2013) 157–162.
[9] J. Jeong, M. Alfreider, R. Konetschnik, D. Kiener, S. Oh, Acta Mater. 158 (2018) 407–421.
[10] Y. Liu, N. Li, M.A. Kumar, S. Pathak, J. Wang, R.J. McCabe, N.A. Mara, C.N. Tome, Acta Mater. 135 (2017) 411–421.
[11] H.J. Yang, S.M. Yin, C.X. Huang, Z.F. Zhang, S.D. Wu, S.X. Li, Y.D. Liu, Adv. Eng. Mater. 10 (10) (2008) 955–960.
[12] M. Bevis, A.G. Crocker, in: Proceedings of the Royal Society of London Series a-Mathematical and Physical Sciences, 304, 1968, p. 123.
[13] M. Bevis, A.G. Crocker, in: Proceedings of the Royal Society of London Series a-Mathematical and Physical Sciences, 313, 1969, p. 509.
[14] D. Ando, J. Koike, Y. Sutou, Mater. Sci. Eng. a-Struct. Mater. Properties Microstruct. Process. 600 (2014) 145–152.
[15] M.R. Barnett, Mater. Sci. Eng. a-Struct. Mater. Properties Microstruct. Process. 464 (1–2) (2007) 1–7.
[16] C.H. Caceres, P. Lukac, A. Blake, Philos. Mag. 88 (7) (2008) 991–1003.
[17] H.D. Fan, S. Aubry, A. Arsenlis, J.A. El-Awady, Acta Mater. 92 (2015) 126–139.
[18] M. Lentz, M. Risse, N. Schaefer, W. Reimers, I.J. Beyerlein, Nat. Commun. 7 (2016) 11068.
[19] I.J. Beyerlein, X.H. Zhang, A. Misra, Annu. Rev. Mater. Res. 44 (44) (2014) 329–363.
[20] B.M. Morrow, R.J. Mccabe, E.K. Cerreta, C.N. Tome, Metallur. Mater. Trans. a-Phys. Metallur. Mater. Sci. 45a (1) (2014) 36–40.
[21] F. Sansoz, H.C. Huang, D.H. Warner, JOM 60 (9) (2008) 79–84.
[22] J. Wang, I.J. Beyerlein, J.P. Hirth, Modell. Simul. Mater. Sci. Eng. 20 (2) (2012).
[23] J. Wang, I.J. Beyerlein, C.N. Tome, Scr. Mater. 63 (7) (2010) 741–746.
[24] Y. Guo, H. Abdolvand, T.B. Britton, A.J. Wilkinson, Acta Mater. 126 (2017) 221–235.
[25] A. Serra, D.J. Bacon, Philosoph. Mag. a-Phys. Condens. Matter. Struct. Defects Mech. Proper. 73 (2) (1996) 333–343.
[26] M.A. Kumar, K. Dang, V. Taupin, R. McCabe, C. Tomé, L. Capolungo, Materialia 23 (2022) 101437.
[27] M.A. Kumar, R. McCabe, C. Tomé, L. Capolungo, Materials Today Commun. 33 (2022) 104634.
[28] M.A. Kumar, R.J. McCabe, V. Taupin, C.N. Tomé, L. Capolungo, Mater. Charact. 194 (2022) 112457.
[29] H. Abdolvand, M. Daymond, C. Mareau, Int. J. Plast. 27 (11) (2011) 1721–1738.
[30] J.H. Cheng, S. Ghosh, J. Mech. Phys. Solids 99 (2017) 512–538.
[31] H.D. Fan, J.A. El-Awady, J. Appl. Mech.-Trans. Asme 82 (10) (2015).
[32] M.S. Hooshmand, M.J. Mills, M. Ghazisaeidi, Modell. Simul. Mater. Sci. Eng. 25 (4) (2017).
[33] M.A. Kumar, I.J. Beyerlein, R.J. McCabe, C.N. Tome, Nat. Commun. 7 (2016) 13826 Article.
[34] M.A. Kumar, A.K. Kanjarla, S.R. Niezgoda, R.A. Lebensohn, C.N. Tome, Acta Mater. 84 (2015) 349–358.
[35] I.J. Beyerlein, M. Arul Kumar, Handbook of Materials Modeling in: S. Andreoni, S. Yip (Eds.), Springer Nature, Switzerland, 2018.

[36] H. Abdolvand, M. Majkut, J. Oddershede, J. Wright, M. Daymond, Acta Mater. 93 (2015) 246–255.
[37] L. Balogh, S.R. Niezgoda, A.K. Kanjarla, D.W. Brown, B. Clausen, W. Liu, C.N. Tome, Acta Mater. 61 (10) (2013) 3612–3620.
[38] T. Bieler, L. Wang, A. Beaudoin, P. Kenesei, U. Lienert, Metallur. Mater. Trans. a-Phys. Metallur. Mater. Sci. 45A (1) (2014) 109–122.
[39] H. El Kadiri, J. Kapil, A.L. Oppedal, L.G. Hector, S.R. Agnew, M. Cherkaoui, S.C. Vogel, Acta Mater. 61 (10) (2013) 3549–3563.
[40] M.A. Kumar, B. Clausen, L. Capolungo, R.J. McCabe, W. Liu, J.Z. Tischler, C.N. Tome, Nat. Commun. 9 (2018) 4761.
[41] M. Lentz, R.S. Coelho, B. Camin, C. Fahrenson, N. Schaefer, S. Selve, T. Link, I.J. Beyerlein, W. Reimers, Mater. Sci. Eng. a-Struct. Mater. Properties Microstruct. Process. 610 (2014) 54–64.
[42] Z.Z. Shi, Y.D. Zhang, F. Wagner, P.A. Juan, S. Berbenni, L. Capolungo, J.S. Lecomte, T. Richeton, Acta Mater. 83 (2015) 17–28.
[43] L. Wang, R.I. Barabash, Y. Yang, T.R. Bieler, M.A. Crimp, P. Eisenlohr, W. Liu, G.E. Ice, Metallur. Mater. Trans. a-Phys. Metallur. Mater. Sci. 42a (3) (2011) 626–635.
[44] R. McCabe, M.A. Kumar, W. Liu, C. Tomé, L. Capolungo, Acta Mater. (2021) 117359.
[45] S. Lay, G. Nouet, Philosoph. Mag. a-Phys. Condens. Matter. Struct. Defects Mech. Proper. 72 (3) (1995) 603–617.
[46] T. Braisaz, P. Ruterana, G. Nouet, R.C. Pond, Philosoph. Mag. a–Phys. Condens. Matter. Struct. Defects Mech. Proper. 75 (4) (1997) 1075–1095.
[47] J. Ye, R.K. Mishra, A.K. Sachdev, A.M. Minor, Scr. Mater. 64 (3) (2011) 292–295.
[48] H. Zhou, G.M. Cheng, X.L. Ma, W.Z. Xu, S.N. Mathaudhu, Q.D. Wang, Y.T. Zhu, Acta Mater. 95 (2015) 20–29.
[49] M.Y. Gong, J.P. Hirth, Y. Liu, Y. Shen, J. Wang, Mater. Res. Lett. 5 (7) (2017) 449–464.
[50] A. Ostapovets, P. Molnar, R. Groger, in: 6th International Conference on Nanomaterials by Severe Plastic Deformation (Nanospd6), 2014, p. 63.
[51] Q. Sun, X.Y. Zhang, J. Tu, Y. Ren, H. Qin, Q. Liu, Philos. Mag. Lett. 95 (3) (2015) 145–151.
[52] Q. Sun, X. Zhang, Y. Ren, L. Tan, J. Tu, Mater. Charact. 109 (2015) 160–163.
[53] J. Tu, X.Y. Zhang, Z.M. Zhou, C. Huang, Mater. Charact. 110 (2015) 39–43.
[54] J. Hirth, J. Wang, C. Tomé, Prog. Mater Sci. 83 (2016) 417–471.
[55] J.T. Lloyd, in: Proceedings of the Royal Society a-Mathematical Physical and Engineering Sciences, 474, 2018.
[56] A. Ostapovets, A. Serra, Philos. Mag. 94 (25) (2014) 2827–2839.
[57] Y. Hu, V. Turlo, I.J. Beyerlein, S. Mahajan, E.J. Lavernia, J.M. Schoenung, T.J. Rupert, Phys. Rev. Lett. 125 (20) (2020) 205503.
[58] Y. Hu, V. Turlo, I.J. Beyerlein, S. Mahajan, E.J. Lavernia, J.M. Schoenung, T.J. Rupert, Acta Mater. 194 (2020) 437–451.
[59] P.E. Marshall, G. Proust, J.T. Rogers, R.J. Mccabe, J. Microsc. 238 (3) (2010) 218–229.
[60] C. Pradalier, P.A. Juan, R.J. McCabe, L. Capolungo, Integr. Mater. Manuf. Innov. 7 (1) (2018) 12–27.
[61] R.A. Lebensohn, A.K. Kanjarla, P. Eisenlohr, Int. J. Plast. 32 (33) (2012) 59–69.
[62] M.A. Kumar, I.J. Beyerlein, C.N. Tome, Acta Mater. 116 (2016) 143–154.
[63] I.J. Beyerlein, C.N. Tome, Int. J. Plast. 24 (5) (2008) 867–895.
[64] G. Simmons, H. Wang, MIT press (1971).
[65] I.J. Beyerlein, R.J. McCabe, C.N. Tome, J. Mech. Phys. Solids 59 (5) (2011) 988–1003.
[66] L. Jiang, M. Gong, J. Wang, Z. Pan, X. Wang, D. Zhang, Y.M. Wang, J. Ciston, A.M. Minor, M. Xu, Nat. Commun. 13 (1) (2022) 1–11.
[67] Y. Liu, P.Z. Tang, M.Y. Gong, R.J. McCabe, J. Wang, C.N. Tomé, Nat. Commun. 10 (2019) 3308.
[68] Y. Liu, N. Li, S. Shao, M. Gong, J. Wang, R.J. McCabe, Y. Jiang, C.N. Tomé, Nat. Commun. 7 (2016) 11577.
[69] A. Luque, M. Ghazisaeidi, W.A. Curtin, Acta Mater. 81 (2014) 442–456.
[70] A. Ostapovets, R. Groger, Modell. Simul. Mater. Sci. Eng. 22 (2) (2014) 025015 Article.
[71] C.D. Barrett, H. El Kadiri, Acta Mater. 70 (2014) 137–161.
[72] J. Wang, S.K. Yadav, J.P. Hirth, C.N. Tome, I.J. Beyerlein, Mater. Res. Lett. 1 (3) (2013) 126–132.
[73] J. Wang, I.J. Beyerlein, J.P. Hirth, C.N. Tome, Acta Mater. 59 (10) (2011) 3990–4001.
[74] L. Jiang, M.A. Kumar, I.J. Beyerlein, X. Wang, D. Zhang, C. Wu, C. Cooper, T.J. Rupert, S. Mahajan, E.J. Lavernia, J.M. Schoenung, Mater. Sci. Eng. 759 (2019) 142–153.
[75] M.A. Kumar, I.J. Beyerlein, R.A. Lebensohn, C.N. Tome, Modell. Simul. Mater. Sci. Eng. 25 (6) (2017) 064007 Article.
[76] M.A. Kumar, I.J. Beyerlein, C.N. Tome, J. Appl. Phys. 120 (15) (2016) 155105.
[77] B. Leu, M.A. Kumar, I.J. Beyerlein, Materialia 17 (2021) 101124.
[78] B. Leu, M.A. Kumar, P.F. Rottmann, K.J. Hemker, I.J. Beyerlein, J. Mater. Eng. Perform. (2022) 1–12.
[79] K. Yaddanapudi, B. Leu, M.A. Kumar, X. Wang, J.M. Schoenung, E.J. Lavernia, T.J. Rupert, I.J. Beyerlein, S. Mahajan, Acta Mater. 204 (2021) 116514.
[80] M.A. Kumar, L. Capolungo, R.J. McCabe, C.N. Tomé, Sci. Rep. 9 (1) (2019) 3846.
[81] C.N. Tomé, M.A. Kumar, J. Graham, K. Dang, Y. Liu, P. Tang, S. Wang, R.J. McCabe, L. Capolungo, in: Magnesium Technology, Springer, 2020, pp. 3–5. 2020.
[82] D.E. Spearot, V. Taupin, K. Dang, L. Capolungo, Mech. Mater. 143 (2020) 103314.
[83] C.D. Barrett, H. El Kadiri, Acta Mater. 63 (2014) 1–15.
[84] W.A.T. Clark, R.H. Wagoner, Z.Y. Shen, T.C. Lee, I.M. Robertson, H.K. Birnbaum, Scr. Metall. Mater. 26 (2) (1992) 203–206.
[85] A. Fernández, A. Jérusalem, I. Gutiérrez-Urrutia, M. Pérez-Prado, Acta Mater. 61 (20) (2013) 7679–7692.
[86] H. Abdolvand, M. Daymond, J. Mech. Phys. Solids 61 (3) (2013) 803–818.
[87] M. Ardeljan, R.J. McCabe, I.J. Beyerlein, M. Knezevic, Comput. Methods Appl. Mech. Eng. 295 (2015) 396–413.
[88] I.J. Beyerlein, C.N. Tome, in: Proceedings of the Royal Society a–Mathematical Physical and Engineering Sciences, 466, 2010, pp. 2517–2544.
[89] S.R. Niezgoda, A.K. Kanjarla, I.J. Beyerlein, C.N. Tome, Int. J. Plast. 56 (2014) 119–138.
[90] M. Wronski, M. Arul Kumar, L. Capolungo, R. Madec, K. Wierzbanowski, C.N. Tome, Mater. Sci. Eng. a-Struct. Mater. Properties Microstruct. Process. 724 (2018) 289–297.